Spin, exchange, and anisotropy in the covalent-chain antiferromagnet $TlFeS_2$

D. Welz* and M. Nishi
Institute for Solid State Physics, University of Tokyo, Roppongi, Minato-ku, Tokyo 106, Japan
(Received 26 September 1991)

Single crystals of the minimally dimerized chain antiferromagnet $TlFeS_2$ have been investigated by thermal neutron diffraction and bulk susceptibility measurements. Collinear order perpendicular to the chain axis appears below a Néel temperature $T_N=196(1)$ K, confirming earlier powder-derived data after correction for an ambiguity in the moment direction. Analysis of the spin-wave dispersion in terms of a classical Heisenberg model, $\mathcal{H}=-2\sum_{\langle ij\rangle}J_{ij}\mathbf{S}_i\cdot\mathbf{S}_j-D\sum_i(S_i^{\parallel})^2$, with a spin $S=0.93$ corresponding to the powder-diffraction ordered moment yields an intrachain exchange constant $J=-55(3)$ meV and interchain-intrachain exchange ratios of order 5×10^{-3}. The magnetic anisotropy $D/|2J|=2.2\times10^{-4}$ is very small, demonstrating spin-orbit cancellation in a half-filled $3d$ shell in spite of a substantial polarization from in-chain Fe-Fe binding being manifest in an anisotropic Van Vleck susceptibility; its unusual easy-axis symmetry normal to the chains, deduced from coincident in-plane and out-of-plane magnon modes, is considered accidental. A combined analysis of spin-wave, susceptibility, and paramagnetic correlation data corroborates a strongly covalency-reduced moment where a local spin close to $S=\frac{3}{2}$ gives rise to conventional quantum fluctuation and renormalization effects, albeit with no obvious indication of the singlet formation predicted for dimerized local-spin chains; this model implies $J\approx-29$ meV. The low-temperature perpendicular susceptibility may indicate a competitive second-neighbor interaction ($\approx12\%$) in the chains.

I. INTRODUCTION

The thallium thioferrate $TlFeS_2$ is a recently characterized[1,2] member of the $AFeS_2$ family of compounds (Table I), the representatives of which contain tightly bound antiferromagnetic chains of edge-linked Fe-S tetrahedra lined up by weakly bound intervening alkali-metal ions (Fig. 1). Minor structural differences, also reflected in their magnetic properties, conveniently allow the compounds to be divided into two groups: (i) isomorphic monoclinic $KFeS_2$ and $RbFeS_2$ with the Fe-S chains lying in the monoclinic plane and ordered moments slightly tilted from the chain axis[3] and (ii), mutually related[1] through a shear distortion around the chain axis, orthorhombic $CsFeS_2$ with no magnetic order down to a magnetocrystalline transition[4] near 70 K and monoclinic $TlFeS_2$ with moments ordering perpendicular to the chains.[2]

In spite of these differences, all the compounds involve formally trivalent iron with an approximately half-filled $3d$ electronic shell. Ordered magnetic moments (Table I) far below the ionic high-spin value of $5\mu_B$, however, indicate a considerable $3d$ delocalization, which has been attributed[2] largely to immediate Fe contact resulting from in-chain Fe distances not much exceeding the atomic separation in metallic Fe (2.48 Å). Although such covalency may entail a substantial axial polarization of the Fe electronic configuration, it should introduce no orbital moment, as the spin-orbit coupling changes sign for half filling regardless of the symmetry of the bonding environment. While the cancellation may hold to lowest order only and further Fe-S covalency may also lead to some $3d$ electron excess, an electron-spin-resonance (ESR) g factor[5] of 2.03 for $KFeS_2$, being close to the spin-only value, nevertheless points to a highly isotropic magnetic character for the compounds. Indeed, only a very small magnetic anisotropy was seen in an inelastic-neutron-scattering investigation[5] of $KFeS_2$.

A delocalization via direct Fe contact might qualify the thioferrate chains as one-dimensional itinerant-electron magnets, irrespective of either a truly metallic ground state or a stabilization by an antiferromagnetic band gap. For the analogous layers of edge-sharing tetrahedra in the tetragonal phase of iron monosulfide, an

TABLE I. Crystallographic and magnetic data for the $AFeS_2$ family of covalent-chain antiferromagnets. Whereas the chains in $KFeS_2$ are magnetically uniform, the structures of the Cs and Tl compounds permit a nonzero dimerization of Fe. $CsFeS_2$ undergoes a first-order magnetocrystalline transition at about 70 K; the high-temperature symmetry is listed here.

Compound	Lattice symmetry	Intrachain Fe separation	T_N	Ordered moment	Ordering direction	Ref.
$KFeS_2$	monoclinic $C2/c$	2.70 Å uniform	250 K	$2.43\mu_B$	13° from chain	3
$CsFeS_2$	orthohombic $Immm$	2.71 Å dimerized		(no order above $T_{struct}\approx70$ K)		4
$TlFeS_2$	monoclinic $C2/m$	2.65 Å dimerized	190 K	$1.85\mu_B$	perpendicular to chain	1,2

electronic-structure calculation[6] has in fact shown that Fe-Fe covalency makes a major contribution to the 3*d*-band width, here even rendering the compound nonmagnetic, and has also indicated a (semi)metallic behavior. Accordingly, the local moments in the present antiferromagnetic chains may significantly depend on their relative orientation; yet this will hardly affect observable thermal-equilibrium properties, as the magnetic susceptibility indicates substantial short-range order up to the decomposition temperature.[7] Of greater relevance is that the associated moment reduction is in principle continuous and may result in an arbitrary [i.e., non-(half-)integer] local spin whose quantization is undefined. In this context, it is interesting to note that the smaller ordered moment observed for $TlFeS_2$ (Table I) correlates with a smaller Fe separation in this compound.

There is yet another interesting aspect. The thioferrate chains in the group (ii) compounds are distinguished by Fe space-group positions that permit a finite dimerization as a result of the particular low symmetry of the Tl or Cs arrangement in these structures (Fig. 1). Although the actual influence [e.g., $z_{Fe}=0.2486(5)$ rather than 0.25 for $CsFeS_2$ (Ref. 8)] is very small owing to the strong intrachain binding forces, quantum effects related to the formation of a singlet state with a finite singlet-triplet excitation gap, as theoretically predicted[9] for localized antiferromagnetic Heisenberg chains with exchange dimerization, cannot be dismissed *a priori* because of the critical dependence of exchange on orbital overlap and the singular evolution of the gap away from the uniform limit. In any case, however, such effects must disappear in the classical limit of large spin quantum numbers S. The chains in the compounds of group (i), on the other hand, show only alternating small lateral displacements of Fe, thus remaining magnetically uniform.

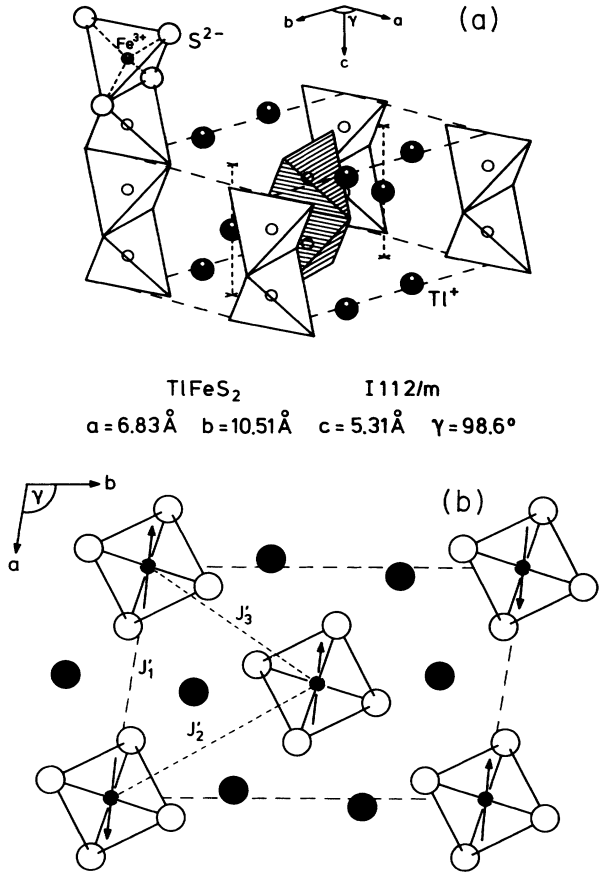

FIG. 1. (a) Crystallographic and (b) magnetic structure of $TlFeS_2$ shown in terms of a nonstandard $I2/m$ cell. According to powder neutron-diffraction data (Ref. 2), ordered moments of $1.85(6)\mu_B$ point in the monoclinic plane 60(10)° away from the shorter diagonal; the sign of the angle has been inverted in the figure to comply with the single-crystal susceptibility of this work.

As the covalency sets the present series of thioferrates apart from the ionic (and mostly uniform) quasi-one-dimensional (quasi-1D) magnets predominantly studied[10,11] (such as the pseudoperovskite $KCuF_3$, the group of hexagonal trihalogenides, or metalorganic systems such as TMMC), a comprehensive investigation is certainly warranted. With the compounds being highly isotropic magnets, the availability of many quantitative theoretical results as well as the significance of quantum effects for localized Heisenberg chains[12] may be utilized to delineate the role of delocalization and probe the interrelation of quantum character and itinerancy. In addition, the possibility of comparing similar compounds with yet partly different attributes within the thioferrate series (Table I) can facilitate a correct interpretation of the measured properties.

We have thus conducted an investigation of $TlFeS_2$ by means of inelastic-neutron-scattering and susceptibility measurements on single crystals. The presentation in this paper is as follows. First, instrumental details are given (Sec. II) and the experimental data described and analyzed (Sec. III). Then the microscopic origin of exchange and anisotropy is discussed (Sec. IV A) and a detailed cross analysis given in terms of a quantum spin model (Sec. IV B). Finally, the principal findings are summarized and put into perspective (Sec. V).

II. EXPERIMENTAL DETAILS

Polycrystalline $TlFeS_2$ was obtained by synthesis from the elements as described earlier.[2] The powder was enclosed in evacuated quartz tubes and lowered through a Bridgman furnace, where the melting point was roughly located at $\approx 600\,^{\circ}C$. No entire single-crystal ingots were obtained in this way, but from 15-mm segments cut normal to the growth (i.e., chain) axis by means of a wheel cutter, large elongated grains with an irregular cross section of about 5×5 mm^2 could be readily isolated by means of a knife and visual inspection. The procedure revealed the crystals to be somewhat delicate: The constituent fibers are strong, but they bend and separate easily. Fresh surfaces have a silver-metallic appearance and slowly darken with exposure to ambient air.

Double- and triple-axis neutron-diffraction data were taken on the PANSI, ND1, and TUNS spectrometers at the JRR-2 reactor of the Japanese Atomic Energy Research Institute. After checking, two crystals of simi-

lar size (about 2 g each) and negligible mosaic spread were oriented for the $(0kl)$ and $(4\eta,k,-3\eta)$ scattering planes, respectively, and mounted in He-filled aluminum containers; these planes contain the lowest and second-lowest magnetic reflections, respectively, and happen to be almost perpendicular to each other (mutual angle 91.6°). In contradistinction to the choice of coordinates in Fig. 1, for indexing we employ a standard $C12/m1$ setting, where b represents the monoclinic chain-axis (Fig. 2), the corresponding x-ray lattice parameters[1] being $a=11.64$ Å, $b=5.31$ Å, $c=10.51$ Å, and $\beta=144.6°$, whence $a^*=0.931$ Å^{-1}, $b^*=1.184$ Å^{-1}, $c^*=1.032$ Å^{-1}, and $\beta^*=35.4°$. All major magnetic reflections then take the form (eoh), while a second set (oeh) is extinct but for nonzero dimerization and omitted from Fig. 2; here e, o, and h denote "even," "odd," and "half integer," respectively. The magnetic ordering direction in the figure is 30° counterclockwise from the c^* axis, where the sign of the angle has been reversed with respect to Ref. 2 to comply with the single-crystal susceptibility of this work (see Sec. III B).

On all instruments, (002) reflecting pyrolytic graphite was used as neutron monochromator and analyzer, and a pyrolytic graphite filter was inserted before the sample for incident energies up to 41 meV inclusive. Inelastic magnon data were collected with segmented variable (PANSI) or monolithic (TUNS) vertically focusing monochromators. In most measurements, 40′ horizontal collimation was used throughout the neutron path, while on TUNS a 60′-30′-30′-60′ sequence had to be taken. Cooling below room temperature was accomplished by a "Displex" closed-cycle He refrigerator mounted on the sample table. Where important, the temperature was monitored with a precalibrated silicon diode (Lake Shore Cryotronics) in thermal contact with the sample container.

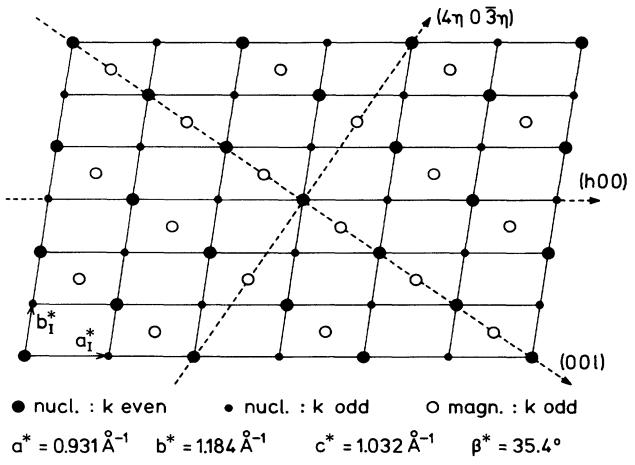

FIG. 2. $TlFeS_2$ reciprocal lattice illustrating the standard $C2/m$ indexing scheme (Ref. 1) employed in this work, with the b axis being in the chain direction. The rhomboid mesh corresponds to the reciprocal $I2/m$ cell of Fig. 1, and the moment orientation is 30° counterclockwise from the $(00l)$ axis. Experiments were performed in the $(0kl)$ and $(4\eta,k,-3\eta)$ scattering planes, which are almost (91.6°) perpendicular to each other.

For analysis (Sec. III A), the magnon data were fitted with a convolution of the theoretical scattering cross section and instrumental resolution function,[13] using a variant of the computer program FIT3AX.[14] The spherical Hartree-Fock result for free Fe^{3+} from Ref. 15 was taken as the magnetic form factor. A background slope and small coordinate offsets were included where thought appropriate; the latter were particularly important for modeling constant-energy scans in the chain direction where the symmetry of the scan profile is sensitive to even minor misorientations of the resolution ellipsoid. As the convolution in FIT3AX is performed numerically, the spin-wave dispersion was artificially broadened in energy in dependence on the scan; this broadening was kept as small as possible [0.6–5 meV full width at half maximum (FWHM)] in order to minimize effects on the fitted parameters, and minor discretization wiggles apparent on some profiles were tolerated.

The magnetic susceptibility below room temperature was recorded in a field of 1 T (10 kG) with a superconducting-quantum-interference-device (SQUID) magnetometer (S.H.E. Corporation) for three orthogonal crystal directions. A smaller sample of about $2\times2\times5$ mm^3 (0.137 g) was used here, the coordinates of which were established by neutron diffraction. To avoid corrections for a sample holder contribution, the crystal was freely suspended on cotton thread where any misorientation is believed to have stayed well within ±10°. While the sample turned out markedly free of paramagnetic impurities, zero-field intercepts revealed a significant [$3.3(1)\times10^{-4}$ cm^3/mol] ferromagnetic background (such as from impurities with $T_c \gg 300$ K), which was assumed to be isotropic and immediately subtracted. Although constant within experimental uncertainty, this background may account for some signal drift observed at lower temperatures; the susceptibility and its anisotropy at room temperature, however, were fully reproducible.

III. RESULTS

A. Neutron scattering

Prior to the inelastic measurements, the $(0,1,\frac{1}{2})$ magnetic Bragg intensity was monitored as a function of temperature in double-axis configuration (Fig. 3). The rounded decrease suggests a conventional second-order transition to three-dimensional (3D) magnetic order. Extrapolation yields a Néel temperature $T_N=196(1)$ K, which improves on the previous 190(10) K obtained by powder Mössbauer spectroscopy,[2] and the range of critical exponents admitted by the final data points, $2\beta=0.66(10)$, is compatible with the theoretical 3D Heisenberg value ($\beta=0.365$).[16] Accordingly, the characteristic critical scattering could be easily observed and showed a surprisingly high inelasticity, even close to T_N, that indicates a very large magnon energy scale.

Magnon data were then taken with a triple-axis setup for a sample temperature of 100 K, i.e., at about $\frac{1}{2}T_N$. Scans in energy up to 40 meV at magnetic zone centers with different reciprocal-lattice offsets revealed only one magnon mode around 5 meV, although for spins ordering

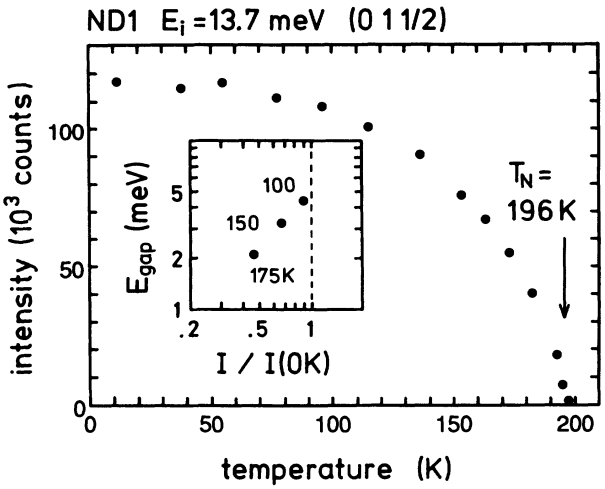

FIG. 3. Temperature dependence of the integrated $(0,1,\frac{1}{2})$ magnetic Bragg intensity, yielding $T_N = 196(1)$ K. The double-logarithmic inset shows the $(0,1,\frac{1}{2})$ magnon gap energy vs magnetic intensity, indicating that the gap varies roughly proportional to the square of the sublattice magnetization.

perpendicular to the chain direction an easy-plane-type anisotropy giving rise to two components, a lower in-plane (IP) and a higher out-of-plane (OP) mode, might rather be expected [compare, e.g., the case of $KCuF_3$ (Ref. 17) or TMMC (Ref. 18)]. Thus our best resolved data (Fig. 4) taken with a low incident energy ($E_i = 13.7$ meV) at the $(0,1,\frac{1}{2})$ position, where the IP intensity dominates 6:1, are in good agreement with a single-mode fitted profile, yielding a gap energy of 4.3(1) meV. The high-energy tail of the profile here again reflects a steep dispersion in the chain direction.

As this suggests a coincidence of IP and OP gap energies and, consequently, an unusual axial symmetry of the anisotropy normal to the chain direction, we analyze two otherwise identical scans taken at the $(0,1,-\frac{1}{2})$ and $(0,1,-\frac{3}{2})$ zone-center positions with an incident energy of 40.5 meV. The data and estimated incoherent scattering and background contributions are shown in Fig. 5 together with FIT3AX simulated profiles based on coincident IP and OP modes at 4.3 meV. The predicted ratio of the scan-integrated intensities, which combines the influence of moment orientation, magnetic form factor, and focusing, results to 1.14, in perfect agreement with the experimental ratio of 1.13(5), whereas neither the IP mode alone with 1.71 nor the OP mode alone with 0.38 can explain the observed variation. We have to conclude that both modes are contained in the 5-meV peaks, the absence of a discernible energy shift between the scans implying that they are degenerate within the data resolution of about 0.5 meV.

In order to further characterize the anisotropy, the temperature dependence of the $(0,1,\frac{1}{2})$ magnon gap below T_N was briefly examined, and the relation between gap energy and magnetic Bragg intensity is shown in the double-logarithmic inset of Fig. 3. The data indicate that the variation with sublattice magnetization between 100 and 175 K follows a M_S^p power law with an exponent

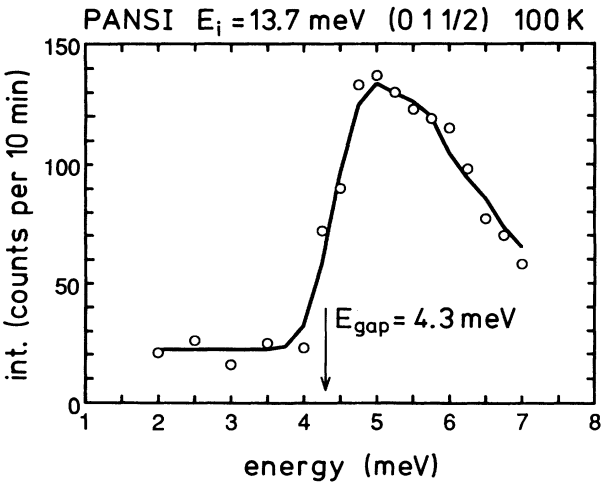

FIG. 4. Energy scan at the $(0,1,\frac{1}{2})$ magnetic zone center and the profile generated by resolution fitting with a single mode (Gaussian broadening 0.6 meV FWHM). The resulting magnon gap energy is 4.3(1) meV at 100 K. The high-energy tail reflects a steep intrachain dispersion; no other mode is found below 40 meV.

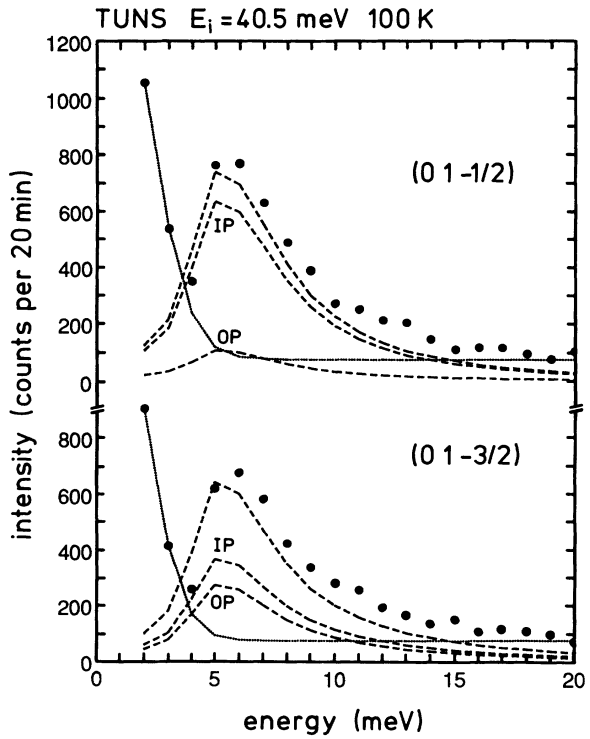

FIG. 5. Magnon gap scans at the $(0,1,-\frac{1}{2})$ and $(0,1,-\frac{3}{2})$ reciprocal-lattice positions. Dotted lines indicate estimated incoherent scattering and background. A simulation (dashed) for coincident in-plane (IP) and out-of-plane (OP) modes at 4.3 meV (Lorentzian broadening 2 meV FWHM) reproduces the measured intensity ratio. The curves have been matched to the data by a common scale factor.

close to $p=2$. An extrapolation to low temperatures then implies a slight ($\approx 7\%$) further increase in the magnon gap below 100 K.

A high incident energy of 83.3 meV was used to probe the steep intrachain dispersion by means of constant-energy scans, where the energy transfer was chosen in dependence on the scan center position such that the long resolution axis extended normal to the scan direction, as attested by the resulting sharp and symmetric double peaks (Fig. 6). However, the energy transfer of 37.9 meV leading to a symmetric experimental profile at $(0,k,\frac{3}{2})$, for instance, differs somewhat from the theoretical prediction[13] implemented in FIT3AX and was also noted to be spectrometer dependent. A likely cause are nonuniformities or mutual correlations in the monochromator and analyzer mosaic spreads, and the associated problems in the resolution fitting were addressed by small coordinate offsets, as mentioned in Sec. II.

The intrachain magnon dispersion shows the typical linear low-energy behavior of antiferromagnets, the resolution fits giving a spin-wave velocity of $\hbar c = 0.54(3)$ eV Å. This is about twice the slope implied by the only other comparable measurement[5] for $KFeS_2$ (≈ 0.26 eV Å), which may therefore be suspected to suffer from some kind of systematic error (a recent experiment[19] at a pulsed neutron source indeed shows a much higher value). In any case, the zone-boundary energy and upper part of the dispersion in $TlFeS_2$ are clearly out of the reach of experiments with thermal reactor neutrons.

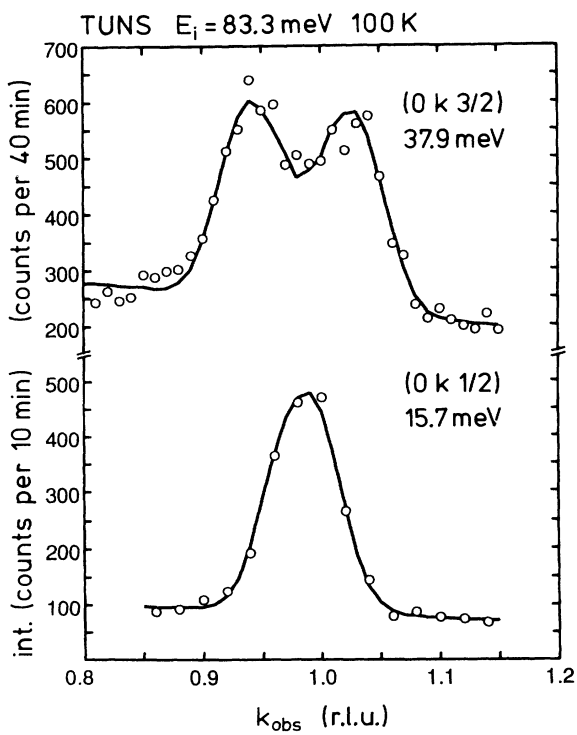

FIG. 6. Constant-energy scans parallel to the chain axis at $(0,k,\frac{3}{2})$ for 37.9 meV and at $(0,k,\frac{1}{2})$ for 15.7 meV transfer, together with resolution fits (Lorentzian broadening 5 meV FWHM). A spin-wave velocity of 0.54(3) eV Å is obtained. The sharp symmetric profiles result from the resolution ellipsoid being oriented normal to the scan direction.

Both constant-energy and constant wave-vector scans with appropriately chosen incident energies were employed to sample the dispersion in the $(00l)$ and $(4\eta,0,-3\eta)$ interchain directions. At the (012) and $(41\bar{3})$ lateral zone boundaries, respectively, the magnon dispersion was thus found to reach an energy of 42.4(5) meV.

The magnon data were analyzed in terms of a customary antiferromagnetic Heisenberg Hamiltonian

$$\mathcal{H} = -2\sum_{\langle ij\rangle} J_{ij}\mathbf{S}_i\cdot\mathbf{S}_j - D\sum_i (S_i^{\parallel})^2 , \tag{1}$$

where the exchange sum with prefactor 2 contains each interacting spin pair exactly once and the anisotropy term with $D>0$ involves the spin ordering direction as easy axis. In the exchange part, we allow for a uniform intrachain coupling J and for three interchain terms J_1', J_2', and J_3', forming a triangle as defined in Fig. 1(b). For the present two-sublattice structure [Fig. 1(b)], standard antiferromagnetic spin-wave theory[20] then gives the dispersion relation

$$\begin{aligned} E(h,k,l) = 2S(\{2(J+J_1'+J_2')-2J_3'[1-\cos(\pi h)]-D\}^2 \\ -[2J\cos(\pi k)+2J_1'\cos(\pi h+2\pi l) \\ +2J_2'\cos(2\pi h+2\pi l)]^2)^{1/2} , \end{aligned} \tag{2}$$

where (hkl) represent the offset from a magnetic zone center.

It should be realized that further couplings, such as between second neighbors in the chains or with components both along and across the chains, cannot be separately inferred from the measured low-energy excitations and that a dimerization in antiferromagnetic chains is even completely hidden in conventional spin-wave theory [$J_{obs} = -(J_1J_2)^{1/2}$].[9] The four interactions in (2) may therefore be regarded as effective parameters that serve to permit a self-contained data description. Similarly, we here simply assume classical spins, so that a quantum renormalization[20] of (2) need not be considered, and accordingly also ignore zero-point motion, taking the spin value S directly from the ordered moment. A refined analysis and combination with paramagnetic correlation and static susceptibility data in Sec. IV B, however, will allow us to go beyond this minimum model.

Using the spin value $S=\frac{1}{2}\mu/\mu_B = 0.925$ corresponding to the low-temperature ordered moment from Ref. 2, the dispersion relation (2) was separately fitted to each magnon scan with respective insensitive parameters fixed and the procedure iterated until all parameters were essentially self-consistent (the fitted profiles include those shown in Figs. 4 and 6). The deconvoluted magnon energies resulting for each scan are given in Fig. 7 together with the theoretical dispersion curves (2) along the $(0k0)$, $(00l)$, and $(4\eta,0,-3\eta)$ reciprocal-space directions, and the corresponding optimized dispersion parameters are listed in Table II. Whereas a well-defined positive value is found for the interchain coupling J_3', as emphasized in Fig. 7 by a dotted line calculated for $J_3'=0$, the interactions J_1' and J_2' cannot be separated in the present two scattering

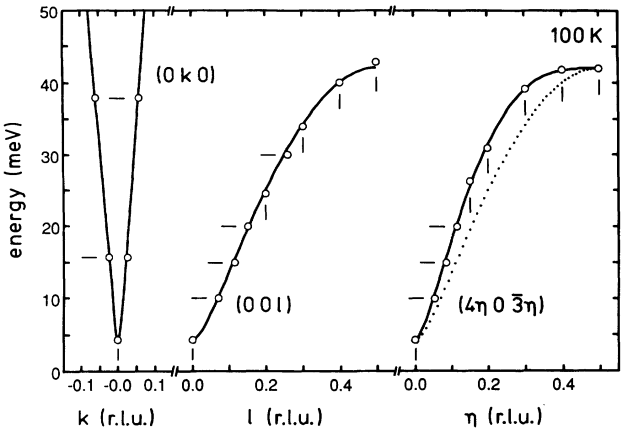

FIG. 7. Magnon energy dispersion at 100 K in the (010), (001), and $(40\bar{3})$ directions from the magnetic zone center, as obtained from resolution fitting. The wave vectors are reduced to the first zone; ticks distinguish constant-energy and constant wave-vector scans. The solid curves are calculated using the relation (2) with the parameters of Table II; the dotted line is the result for $J_3'=0$.

planes and only their sum is obtained. Owing to the thermal renormalization of the gap energy, the present value of D for 100 K should slightly ($\approx 14\%$) underestimate the true parameter in the Hamiltonian (1). This does not apply to $J_1'+J_2'$ and J_3', however, since results for $KCuF_3$,[17] $CsNiCl_3$,[21] and $CsMnCl_3\cdot 2H_2O$ (Ref. 22) have shown that, away from the magnetic zone center, the renormalization in quasi-1D antiferromagnets is small up to T_N.

To examine the intrachain magnetic correlations above the ordering temperature (Fig. 8), a double-axis setup with 30.5 meV incident energy was used. Scans were performed at room temperature and 250 K across the $k=1$ plane at $(0,1,-0.181)$, which ensures that the energy integration in the detector involves just scattering from this plane. From fitting with a 1D Lorentzian convoluted with the appropriately projected Gaussian resolution, which was experimentally derived from the nearby (020) nuclear reflection, the 1D magnetic correlation lengths[11] ξ(293 K)=29(4) Å [or 11(1) spins] and ξ(250 K)=37(5) Å [or 14(2) spins] are obtained.

TABLE II. Exchange and anisotropy parameters in a classical Heisenberg model for $TlFeS_2$, derived from magnon energies at 100 K using the unrenormalized dispersion relation (2) with a spin value $S=0.925$ corresponding to the low-temperature ordered moment (Ref. 2). Because of the thermal renormalization of magnon energies, D should be slightly reduced relative to the value at 0 K. J_1' and J_2' are inseparable in the present scattering planes.

J	$J'=(J_1'+J_2')/2$	J_3'	D(100 K)
−55(3) meV	−0.29(2) meV	+0.13(2) meV	0.024(2) meV

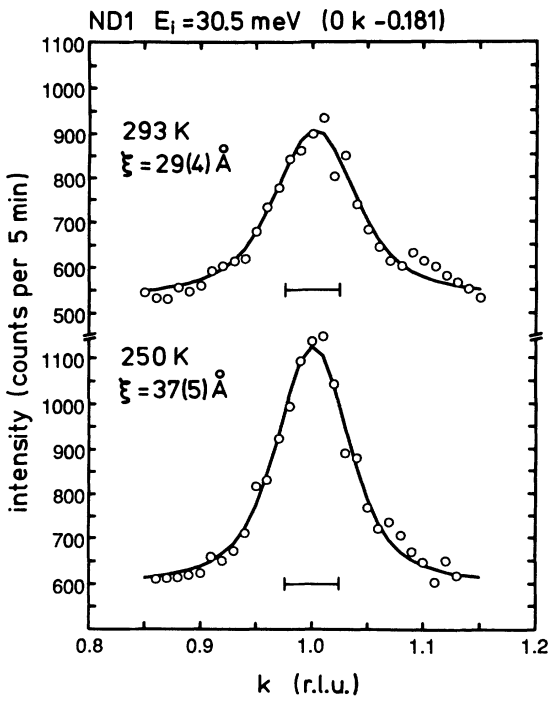

FIG. 8. Energy integrating double-axis scans above T_N across the $k=1$ magnetic plane at $(0,1,-0.181)$, with the integration confined to the plane. The fitting of Lorentzian profiles folded with the Gaussian resolution ($0.049b^*$ FWHM) yields the intrachain correlation lengths 29(4) Å [11(1) spins] at 293 K and 37(5) Å [14(2) spins] at 250 K.

B. Susceptibility measurements

Figure 9 shows the magnetic susceptibility of single-crystal $TlFeS_2$ for three orthogonal field directions: along the chain axis, along the magnetic ordering direction, and

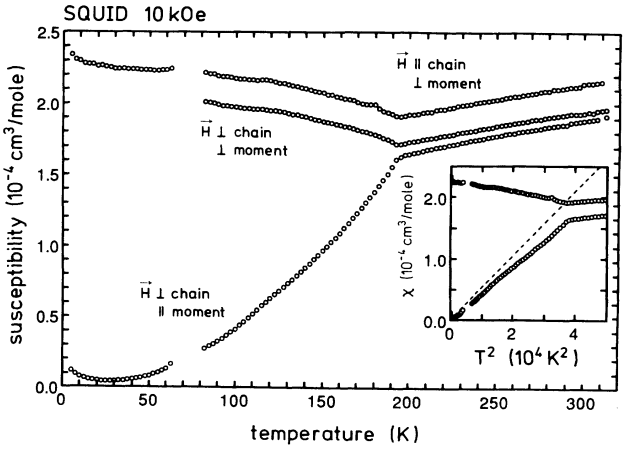

FIG. 9. Single-crystal molar susceptibility of $TlFeS_2$ along three orthogonal axes in an applied field of 1 T (10 kG), after correction for ferromagnetic impurities. A constant offset of the upper curve is attributed to an anisotropic Van Vleck term, which in the parallel susceptibility is virtually compensated by core diamagnetism. The inset highlights the spin-wave T^2 law, the dashed slope being a prediction from the magnon energies for $J_1'=J_2'$.

perpendicular to both. The data exhibit the behavior expected of a nearly isotropic quasi-1D antiferromagnet undergoing 3D collinear order, the order giving rise to a splitting into parallel and perpendicular susceptibility components. There is, however, a peculiar constant offset of $0.20(2)\times10^{-4}$ cm^3/mol between the upper two traces, the origin of which will be discussed in Sec. IV A.

During an initial check of the dependence of the Néel-state splitting on crystal orientation, it became evident that the actual moment direction corresponds to the previous powder neutron-diffraction result[2] mirrored in the monoclinic plane on the $C2/m$ a axis [the shorter diagonal in Fig. 1(b)]. Yet, although the old sign of the angle with this axis must be inverted, the old magnitude (60°) is excellently confirmed, and the moment value ($1.85\mu_B$) is likewise not affected, as both orientations prove to be virtually equivalent in an analysis[2] relying basically on the $(0,1,\frac{1}{2})$ and $(2,1,-\frac{3}{2})$ magnetic intensities alone. In fact, with the $(0kl)$ and $(4\eta,k,-3\eta)$ scattering planes being almost perpendicular (Fig. 2), the revision has no discernible effect on the magnetic intensities in these planes in general. The corrected moment direction is shown in Fig. 1(b).

With values of the order 2×10^{-4} cm^3/mol, the present single-crystal susceptibility falls well below an earlier powder measurement[2] ($\approx9\times10^{-4}$ cm^3/mol), suggesting a considerable impurity contribution to the latter (this effect, also pointed out[23] for $KFeS_2$ seems to plague powder susceptibility measurements of the chain thioferrates in general). As demonstrated by the χ-versus-T^2 inset of Fig. 9, the parallel and perpendicular susceptibilities below the ordering temperature are in reasonable agreement with a simple T^2 law practically up to T_N, the overall slope coefficients above 80 K being $+4.3(2)\times10^{-9}$ and $-0.9(1)\times10^{-9}$ cm^3/(mol K^2), respectively. The Néel temperature implied by the susceptibility data is consistent with the more accurate result from the magnetic Bragg intensity.

IV. DISCUSSION

A. Microscopic origins

1. Exchange interaction

A markedly anisotropic magnon dispersion (Fig. 7) corresponding to the exchange parameter relation $|J|\gg|J'|$ (Table II) unambiguously establishes $TlFeS_2$ as a quasi-1D magnetic system, the property being here primarily attributable to a very strong interaction within the thioferrate chains. Accordingly, an upward continuation of the dispersion by the relation (2) predicts a 1D zone-boundary energy (neglecting J' and D) of $E(0,\frac{1}{2},0)=4S|J|=204(11)$ meV that, along with similar values[19] to be expected for the alkali-metal relatives, may well be the highest for 1D systems to date. The present intrachain exchange constant $J=-55(3)$ meV for a classical $S=0.93$ is far above the value $J=+15$ meV in bcc metallic iron ($S=1.11$),[24] but it is rivaled or surpassed in other chalcogenides, as, for instance, by $J=-87(13)$ meV in hexagonal NiS ($S=1$) (Ref. 25) [J values as defined by Eq. (1)].

According to the Goodenough-Kanamori rules[26] for cations with half-filled shells, both Fe-Fe direct and Fe-S-Fe indirect exchange interactions in the thioferrate chains should be antiferromagnetic. Yet, while exchange of the present magnitude may in general reflect covalent bonding contributions of any kind, it here supports the concept of Fe-Fe contact. This is seen by estimating the Fe-S-Fe contribution from the exchange in the blende-superlattice compound chalcopyrite ($Cu^+Fe^{3+}S_2^{2-}$), where merely corner-sharing tetrahedra preclude any Fe overlap: Applying the molecular-field formula $kT_N=\frac{2}{3}S(S+1)z|J|$ for the Néel temperature of a 3D antiferromagnet[20] to the experimental data $T_N\approx825$ K,[27] $\mu=3.85\mu_B$,[28] and $z=4$, we find $J\approx-5$ meV for a single Fe-S-Fe path, which after doubling for edge-sharing tetrahedra still represents only a smaller part of the result for the thioferrate chains, even if quantum corrections are taken into account (Sec. IV B).

Reaching above 40 meV, the interchain dispersion in the Tl thioferrate alone exceeds the 1D dispersion of most ionic chain magnets, but being proportional to $(|J|\,|J'|)^{1/2}$ it does so mainly because of amplification by the intrachain exchange. Thus the magnitude of the interchain coupling itself is not unusual for the ionic superexchange path involved and more than two orders below the covalent intrachain coupling; if the minor J'_3 is neglected in forming a mean interchain exchange $J'=(J'_1+J'_2)/2=-0.29$ meV, a ratio $|J'/J|=5\times10^{-3}$ is obtained as an approximate measure of the 1D character. Whereas significantly "better" ratios are found especially in metalorganic chain systems, this puts $TlFeS_2$ (like $KFeS_2$ (Ref. 5)] into one class with many simple ionic quasi-1D magnets such as the pseudoperovskite $KCuF_3$ ($|J'/J|=1.0\times10^{-2}$) (Ref. 17) or hexagonal $CsNiCl_3$ ($|J'/J|=1.7\times10^{-2}$).[21]

The present magnon and single-crystal susceptibility data fully corroborate a collinear magnetic structure of $TlFeS_2$. A stable collinear state means that the range of values permitted for the unseparated exchange parameters J'_1 and J'_2 is restricted; on a triangular lattice with positive $J'_3=+0.13$ meV and negative $J'_1+J'_2=-0.58$ meV, the stability criterion $J'_1J'_2-J'_1J'_3-J'_2J'_3>0$ is satisfied only if -0.69 meV$<J'_1, J'_2<+0.11$ meV. In Sec. IV B both interactions will actually be seen to be comparable, as only the choice $J'_1\approx J'_2\approx-0.29$ meV accounts for the coefficient of the T^2 term in the parallel susceptibility. Alternatively, a high degree of stability of the collinear state may be inferred from the experimental ordering temperature being close to the value predicted by the Oguchi relation[29] $kT_N\approx2.1S(S+1)(|J|\,|J'|)^{1/2}$ if $J'=(J'_1+J'_2)/2$ is taken and J'_3 neglected.

2. Anisotropy energy

Compared with exchange, the anisotropy energy in $TlFeS_2$ is very small, $D/|2J|=H_A/H_E=2.2\times10^{-4}$, signifying an excellent realization with $S>\frac{1}{2}$ of a magnetically isotropic system in a low-symmetry structure. Along with $KFeS_2$,[5] the compound in this respect com-

pares favorably, for instance, with the quasi-1D antiferromagnet TMMC ($D/|2J|=-8.6\times10^{-3}$),[18] which is often used as a model Heisenberg system. As pointed out in the Introduction a negligible anisotropy in the thioferrate chains has in fact to be expected, even for a nonspherical low-spin configuration of Fe, as long as a cancellation of spin-orbit coupling takes place in an approximately electron-hole-symmetric $3d^5$ shell, eliminating[30] any significant anisotropy of Fe-Fe exchange as well as of single-site origin. The dependence of moment orientation on differences in the 3D crystal structure (Table I) and the unusual perpendicular easy-axis character of the anisotropy in $TlFeS_2$ indeed imply that effects local to the chains are not invariably predominant.

This, however, leaves the role of the ever-present dipolar magnetic interactions to be clarified, which in antiferromagnetic chains lead to an easy-plane anisotropy with a finite OP magnon gap energy of

$$E_\Gamma=4S\left[3|J|(g\mu_B)^2\sum_n(-1)^{n-1}/(nd)^3\right]^{1/2},$$

where d stands for the 1D lattice spacing (a full 3D lattice summation for $TlFeS_2$ introduces only $\pm2\%$ deviation from 1D symmetry). With $E_\Gamma=4.8$ meV for the Tl thioferrate, the dipolar term alone accounts remarkably well for the measured gap energy, but the correspondence is certainly fortuitous, as the IP gap does not nearly vanish experimentally. In view of the crucial influence of extra-chain contributions (such as from anisotropic interchain exchange), it may be suspected that the dipolar anisotropy is attenuated by a small easy-axis effect in the chains (which may vary with Fe-Fe distance). Here, in particular, single-site or Fe-Fe exchange terms from an uncompensated spin-orbit coupling in a slightly more than half-filled $3d$ shell could occur as a result of Fe-S covalent electron backdonation, as also suggested by an ESR g factor[5] slightly above 2 for $KFeS_2$. In any case, the IP-OP degeneracy in $TlFeS_2$ appears to be purely accidental.

According to antiferromagnetic resonance theory,[31,32] the temperature dependence of the magnon gap energy may be expressed as $E_\Gamma(T)=[2K(T)/\chi_\perp(T)]^{1/2}$. If the anisotropy constant obeys a Zener relation[33] $K(T)\propto M_s(T)^{l(l+1)/2}$, with l being the order of the spherical harmonic associated with the anisotropy energy, and if the variation in the perpendicular susceptibility $\chi_\perp(T)$ can be neglected, a simple power law $E_\Gamma\propto M_s^p$ follows, with $p=\frac{3}{2}$ for a second-order harmonic. For various simple 3D systems[34] with $l=2$, this was found to account for experimental observation up to temperatures as high as 0.6–$0.9T_N$, regardless of the microscopic origin of anisotropy or the functional form of $M_s(T)$. A somewhat faster decay with $p\approx2$ in $TlFeS_2$ (Fig. 3) then also appears to be basically indicative of a second-order anisotropy ($\chi_\perp$ changes by less than 10% between 100 and 175 K), while the deviation from $p=\frac{3}{2}$ may reflect a higher-order ($l=4$) contribution or here signal a breakdown of the Zener relation at higher temperatures. The present decay is clearly at variance with the simple molecular-field prediction $p=1$ for interaction-derived anisotropies.[32]

3. *Susceptibility anisotropy*

We finally turn to the distinct anisotropy in the measured susceptibility (Fig. 9). The offset between the perpendicular susceptibilities along and across the chains (upper two traces) is obviously unrelated to the anisotropy of the spin system, as it persists unchanged into the ordered state and as the susceptibility splitting above T_N does not correspond with the easy-axis symmetry inferred from the magnon modes. An inspection of the difference susceptibility further reveals no indication of a kink at the transition point, thereby precluding a multiplicative g-factor anisotropy and implying a temperature-independent additive term instead that is anisotropic. Possible effects of Fermi-level electrons discounted, a constant susceptibility contribution may arise from the Langevin diamagnetism of atomic cores and the Van Vleck (high-frequency) paramagnetism of valence shells, the latter of which can easily be anisotropic. In contrast, the smaller and slightly decreasing separation above T_N of the parallel and perpendicular susceptibilities across the chains (lower two traces) should reflect the anisotropy of the antiferromagnetic spin system.

The diagonal components of the Van Vleck susceptibility for a single ion may be written[35]

$$\chi_{\eta\eta}^{VV}=2N\mu_B^2\sum_n\frac{|\langle n|L_\eta|0\rangle|^2}{E_n-E_0}\quad(\eta=x,y,z),\tag{3}$$

where L_η are the components of orbital angular momentum, $|0\rangle$ represents the electronic ground state with energy E_0, and $|n\rangle$ are excited configurations of energy E_n (the expression is also applicable to delocalized band states if n is taken to enumerate single-electron excitations[30]). For a $3d^5$ shell in a tetrahedral bonding environment, the only relevant matrix elements are those between occupied e and unoccupied t_2 orbitals of same spin. Thus, while an $S=\frac{5}{2}$ high-spin configuration simply has $\chi^{VV}=0$, an $e^4t_2^1$ ($S=\frac{1}{2}$) low-spin case gives[35] $\chi^{VV}=\frac{40}{3}N\mu_B^2/\Delta E$ and a hypothetical $e^3t_2^2$ ($S=\frac{3}{2}$) case $\frac{20}{3}N\mu_B^2/\Delta E$. Taking the last to be a reasonable approximation for $TlFeS_2$ (compare Sec. IV B), with the e-t_2 splitting from the electronic band structure of tetrahedral iron monosulfides,[6] $\Delta E\approx0.2$ Ry (≈2.7 eV), we obtain the isotropic estimate $\chi^{VV}\approx0.8\times10^{-4}$ cm^3/mol. Incidentally, this is just the order to be expected of core diamagnetism, in accordance with the observation that the low-temperature parallel susceptibility approaches zero (Fig. 9). Moreover, the measured anisotropy of $0.20(2)\times10^{-4}$ cm^3/mol is now seen to represent roughly 25% of the total Van Vleck susceptibility.

In order to account for the anisotropy, a level splitting from Fe-Fe bonding interactions in the chains must be introduced. As also proposed in Ref. 2, here primarily a splitting of $3z^2$-r^2 into bonding and antibonding orbitals can be expected, causing a population loss from the antibonding orbitals (z axis along the chain). From the relations

$$L_x|x^2-y^2\rangle=-i|yz\rangle,\quad L_x|3z^2-r^2\rangle=-\sqrt{3}i|yz\rangle\ ,$$
$$L_y|x^2-y^2\rangle=-i|xz\rangle,\quad L_y|3z^2-r^2\rangle=\sqrt{3}i|xz\rangle\ ,$$
$$L_z|x^2-y^2\rangle=2i|xy\rangle,\quad L_z|3z^2-r^2\rangle=0\ ,$$

it follows that both an increased energy separation for $3z^2$-r^2 bonding orbitals and a population imbalance toward x^2-y^2 orbitals give rise to $\chi_{zz}^{VV}>\chi_{xx}^{VV}=\chi_{yy}^{VV}$, as found experimentally. The anisotropy in the Van Vleck susceptibility forms a striking contrast with the extreme isotropy of the spin system, yet both experimental findings are equally characteristic of a nonspherical low-spin state of electron-hole symmetric Fe^{3+} in the Fe-S chains of $TlFeS_2$.

B. Combined analysis

For the sake of simplicity, in Sec. III A the magnon dispersion of $TlFeS_2$ has been analyzed in terms of localized classical spins and a limited set of phenomenological interactions. With a view to identify a possibly more accurate description, we shall now examine how quantum effects might enter the interpretation and effect the model parameters, and then introduce the correlation and susceptibility data into the analysis. The cross analysis provides a means to refine the Hamiltonian and to test the validity of a local-moment description, including standard spin-wave theory, for this covalent delocalized system.

1. *Quantum corrections*

For localized quantum spins in quasi-1D antiferromagnets, appreciable zero-point fluctuations are expected,[20] leading to a corresponding reduction in the measurable ordered moment, $\mu=g\mu_B(S-\Delta S)$. Linear spin-wave theory here even predicts[36] a divergent reduction for the limit of free chains with zero anisotropy and in this context was little trusted at first.[10] The unphysical behavior, however, can be rectified by taking "kinematical interaction" terms into account[37] (the improved estimate extrapolates to $\mu=0$), revealing the original result to be already reasonably accurate if the spin number is not too small and the system not too close to the 1D isotropic limit. Because the reduction in real systems is not easy to separate from covalency effects, precise experimental values are difficult to obtain, but the data available for highly ionic chain antiferromagnets such as $KCuF_3$ ($S=\frac{1}{2}$) (Refs. 38 and 17) and K_2FeF_5 or Rb_2FeF_5 ($S=\frac{5}{2}$) (Refs. 39 and 40) confirm the soundness of the improved spin-wave prediction.

Applying the linear spin-wave prediction[20] to our interaction model (1) for $TlFeS_2$, we find for the leading term of the spin reduction in the limit $|J'|\ll|J|$, $D\ll|J|$ by suitable expansion of the integrand

$$\Delta S=\frac{1}{2V_{BZ}}\int_{BZ}\left[\frac{2S\{-2(J+J_1'+J_2')+2J_3'[1-\cos(\pi h)]+D\}}{E(h,k,l)}-1\right]dV_{BZ}$$
$$\approx\frac{1}{2\pi}\ln\left[\frac{-16J}{-2(J_1'+J_2')+2J_3'+D}\right]-\frac{1}{2}+0.035\ , \tag{4}$$

where $E(h,k,l)$ is given by (2), the integration extends over one magnetic Brillouin zone (BZ), the small numerical constant has been evaluated for $J_1'=J_2'$, $J_3'=0$, $D=0$, and where the omitted higher-order terms carry prefactors J'/J or D/J. From Table II the moment stabilization in $TlFeS_2$ is governed by the interchain coupling, the data yielding $\Delta S\approx0.56$ and, with the ordered moment from Ref. 2, an intrinsic spin $S\approx0.93+0.56\approx1.49$. Note that (4) is independent of S and also not affected by using a wrong S in the magnon data analysis. Moreover, the kinematical correction[37] turns out to be insignificant, as it decreases ΔS by merely

$$(2S+1)(\Delta S)^{2S+1}/[(1+\Delta S)^{2S+1}-(\Delta S)^{2S+1}]\approx0.07\ .$$

Interestingly, the spin for the Tl thioferrate comes out close to the half-integer value $S=\frac{3}{2}$, even though covalency may give rise to an arbitrary reduction from the ionic spin $\frac{5}{2}$. In any case, the result makes explicit the contrast with the ionic systems $KCuF_3$ and K_2FeF_5, where zero-point fluctuations alone essentially explain the observed low moments.

An additional moment reduction may be anticipated for quantum systems predisposed to form a singlet state, such as quasi-1D antiferromagnets featuring dimerized or integer-spin (Haldane) chains[9,12] and, perhaps also, 2D frustrated arrangements of chains, tentative experimental candidates being the antiferromagnetic triangular lattices of $S=1$ chains in $CsNiCl_3$ (Ref. 41) and $S=\frac{3}{2}$ chains in $CsVCl_3$.[42] However, as a low moment in the present collinear, albeit slightly dimerized, system is readily accounted for by covalency (which is attested by a Van Vleck susceptibility term) and as the behavior of spins with $S\geq\frac{3}{2}$ should be "quasiclassical," only a comparatively small ($\Delta S\ll0.5$) singlet-state-related reduction is conceivable, provided that it survives the electron delocalization. In the following we shall therefore examine a quantum description with a covalency-reduced intrinsic spin $S\approx\frac{3}{2}$ for $TlFeS_2$.

Quantum antiferromagnets differ from a classical system also in an upward renormalization of the magnon energies [Eq. (2)]. Thus, for chains of local $S=\frac{3}{2}$ spins, conventional spin-wave theory[20] predicts a uniform multipli-

cative renormalization by 1.12, while simple $1/S$ scaling of the exact[20] des Cloizeaux–Pearson factor $\pi/2$ for $S=\frac{1}{2}$ gives 1.19 for $S=\frac{3}{2}$ (for $S=1$, this kind of estimate seems to be favored by recent Monte Carlo data[43] after adjusting for finite-size effects). This and the higher quantum spin value imply a downward revision of the magnon-derived exchange constant from the value obtained in a classical framework; with $S=\frac{3}{2}$ and a renormalization of 1.19, instead of an intrachain exchange of -55 meV we find $J\approx-29$ meV from the dispersion slope of $TlFeS_2$.

2. Paramagnetic correlation

From Fisher's solution, the correlation length of a classical Heisenberg chain in units of the spin separation is[11]

$$\xi=\left\{-\ln\left[\coth\left[\frac{2S^2|J|}{kT}\right]-\left[\frac{2S^2|J|}{kT}\right]^{-1}\right]\right\}^{-1}\approx\frac{2S^2|J|}{kT}\ , \tag{5}$$

where the second form holds for $kT\ll 2S^2|J|$. With the $TlFeS_2$ classical spin $S=0.93$ and exchange $J=-55$ meV, this falls short of the measured paramagnetic intrachain correlation (Fig. 8) by a factor of about 3. The discrepancy, however, becomes smaller for an $S=\frac{3}{2}$ quantum model with $J=-29$ meV, and it is particularly diminished if the quantum character is introduced into (5) via the semiempirical substitution $S^2\rightarrow S(S+1)$. In view of a probable overestimation of the measured correlation from the one-sided truncation of the energy integration at the incident neutron energy E_i (which should not be too serious for $E_i=30.5$ meV$\approx kT$) and a possible small enhancement from interchain coupling, the agreement (within a factor 1.5) has then to be considered satisfactory. Rather than the classical model, the correlation length thus corroborates a localized quantum description of the magnetic moments in the Tl thioferrate.

3. Perpendicular susceptibility

The perpendicular Néel-state susceptibility of $TlFeS_2$ from the central data trace in Fig. 9 extrapolates to a low-temperature value of $\approx 2.1\times10^{-4}$ cm^3/mol. With the molecular-field result for a chain of classical moments,[20]

$$\chi_\perp(0\text{ K})=\frac{M_s}{H_E}=N\frac{(g\mu_B)^2}{8|J|}\ , \tag{6}$$

this implies an exchange constant $J\approx-77$ meV that significantly exceeds the magnon-derived result $J=-55(3)$ meV for a classical $S=0.93$. Here the discrepancy cannot be resolved by quantum corrections in the framework of standard spin-wave theory, as may be most easily realized in terms of the sublattice magnetization M_s and an exchange field H_E:[20] A zero-point reduction in M_s and a renormalization of H_E do not affect the consistency of measured ordered moment ($\propto M_S$), magnon energies ($\propto H_E$), and perpendicular susceptibility ($\propto M_s/H_E$). Indeed, first-principles spin-wave operator expansions[44] (for 3D cubic antiferromagnets) confirm the cancellation at least to first order in $1/S$, i.e., for moderate renormalization, and for quasi-2D ionic systems the predicted renormalization of $\chi_\perp$ could be shown[10] to agree with experiment down to about 50% of the molecular-field value.

Thus, for a pure local-moment model, the perpendicular susceptibility of $TlFeS_2$ should indicate that the canting of sublattices is harder than expected from the magnon energies. A possible cause is a next-nearest-neighbor (i.e., intrasublattice) interaction in the chains that softens spin waves but does not affect the susceptibility (which feels intersublattice exchange only). With J_1 and J_2 denoting the interaction between first and second neighbors, respectively, the effect on the low-energy (i.e., long-wavelength) magnons may be expressed by an effective intrachain exchange $J_{\text{eff}}=-[J_1(J_1-4J_2)]^{1/2}$, where magnon and susceptibility data combined imply $J_1\approx-77$ meV and $J_2\approx-9$ meV. Since only J_1 enters the lateral $(h0l)$ dispersion, the values for $J_1'+J_2'$, J_3', and D in Table II must then be scaled by a factor $J_{\text{eff}}/J_1\approx0.7$, but with the new zone-boundary energy being $4S|J_1-2J_2|$ the extrapolated 1D dispersion is almost unchanged. It is not clear, however, to what extent such an interpretation can be trusted, and we ignore possible repercussions on the preceding analysis (a noticeable increase may be anticipated for ΔS). In any case, it seems reasonable to view the effect as a manifestation of electronic delocalization in the thioferrate chains.

4. Parallel susceptibility

The experimental T^2 behavior of the parallel susceptibility (Fig. 9) suggests to evaluate the low-temperature behavior from spin-wave theory.[36] Neglecting anisotropy, taking the limit $|J|\gg|J'|$ in a small-k approximation to the dispersion (2), and extending the integration to infinity, we arrive at

$$\chi_\parallel=\frac{N(g\mu_B)^2}{4kT}\frac{1}{V_{\text{BZ}}}\int_{\text{BZ}}\left[\sinh\left[\frac{E(h,k,l)}{2kT}\right]\right]^{-2}dV_{\text{BZ}}$$
$$\approx\frac{N(g\mu_B)^2(kT)^2}{192S^3|J|^2J'_{\text{eff}}}\ , \tag{7}$$

with

$$J'_{\text{eff}}=\sqrt{J_1'J_2'-J_1'J_3'-J_2'J_3'}\ ,$$

which holds as long as thermal occupation remains in the range of linear dispersion and also well within the Brillouin zone, i.e., up to $2kT\approx25$ meV (see Fig. 7). Because (7) involves just the actual magnon energies [in the forms $S|J|$ and $S(|J|\,|J'|)^{1/2}$], the neglect of quantum renormalization, the use of effective parameters, or a wrong value assumed for S should have no effect if the parameter set does in the same context account for the measured dispersion.

With the choice $J_1'=J_2'$, which yields the maximum value of J'_{eff}, from the data of Table II a smallest possible coefficient

$$\frac{d\chi_{\parallel}}{dT^2}=5.2(3)\times10^{-9}\ \mathrm{cm}^3/(\mathrm{mol\,K}^2)$$

obtains that nevertheless somewhat exceeds the overall experimental result (Fig. 9). This, however, should be attributed to the approximations in the integral (7), and at lower temperatures (i.e., around 100 K; below ≈ 50 K the anisotropy is expected to become dominant) the difference in slope is insignificant in consideration of the present data quality and parameter uncertainties. We may conclude that, for the relation (2) to reproduce the full 2D interchain dispersion, J'_{eff} must be close to its maximum value, which implies that the unseparated interchain interactions J'_1 and J'_2 are comparable and both nonpositive.

A similar low-temperature law may be derived for the perpendicular susceptibility,[44,20] the T^2 term of which simply follows the saturation magnetization while higher orders are much reduced. For the restricted classical dispersion (2), the T^2 term may be expressed as $\chi_{\perp}(0)-\chi_{\perp}(T)=\frac{1}{4}\chi_{\parallel}(T)$, where $\chi_{\parallel}$ is given by (7). Here the simple factor $\frac{1}{4}$ applies strictly only if quantum renormalization and intrasublattice interactions (such as between second neighbors in the chains) can be neglected, but for $TlFeS_2$ this result of spin-wave theory reasonably conforms with experiment (Fig. 9).

5. *Paramagnetic susceptibility*

In the paramagnetic state, the susceptibility of quasi-1D Heisenberg antiferromagnets exhibits[10] a broad maximum at a finite temperature, $T_{\max}$. For the $TlFeS_2$ classical spin $S=0.93$ and exchange $J=-55$ meV, from Fisher's solution for a classical chain[11] we find $T_{\max}\approx 0.95S^2|J|/k\approx 520$ K, while for a quantum chain with $S=\frac{3}{2}$, $J=-29$ meV a much higher[10] $T_{\max}\approx 4.75|J|/k\approx 1600$ K is anticipated. Clearly, the peak temperature lends itself to an immediate identification of the proper spin model, but the relatively low melting points of the chain thioferrates (≈ 900 K for $TlFeS_2$), possibly preceded by decomposition (600–700 K for the alkali-metal compounds[7]) make the truly paramagnetic range inaccessible and apparently[7] preclude an experimental determination of the susceptibility maximum. Even though no decision can be reached from the present, still more limited, data, in view of the support from the 1D magnetic correlation length for $TlFeS_2$ it is here of interest to examine some implications arising specifically for the quantum case.

The maximum susceptibility value predicted[10] for the $S=\frac{3}{2}$ quantum model,

$$\chi_{\max}\approx 0.091N(g\mu_B)^2/|J|\approx 4.0\times10^{-4}\ \mathrm{cm}^3/\mathrm{mol}\ ,$$

is compatible with a smooth data extrapolation to ≈ 1600 K (Fig. 9) and at the same time much higher than implied by the $\chi_{\max}/\chi(0\ \mathrm{K})$ ratios for isolated "gapless" (i.e., nondimerized, half-integer spin) chains,[12] which range from 1.20 for classical spins to 1.45 for $S=\frac{1}{2}$. A similar effect has been inferred[23] for the (nondimerized) K compound from an excessive slope of the powder susceptibility above T_N and was tentatively attributed to a zero-point spin reduction. In fact, on account of a continuous connection with the ordered state, a low-temperature depression in the paramagnetic susceptibility can be expected from any source capable of reducing the perpendicular Néel-state susceptibility relative to $\chi_{\max}$; according to the foregoing analysis, these are primarily a zero-point reduction in M_s (via $\chi_{\perp}=M_s/H_E$) and a competitive second-neighbor coupling (presuming $\chi_{\max}$ to correspond roughly to $J_{\mathrm{eff}}=J_1-2J_2$). Since a second-neighbor coupling of the order 12% in $TlFeS_2$ may hardly account for all of the putative depression, zero-point fluctuations ($\Delta S/S\approx 0.35$) should play a significant role indeed.

It is thus seen that a localized $S\approx\frac{3}{2}$ quantum model yields a satisfactory description of the data available for $TlFeS_2$. We should therefore finally try to clarify one seemingly paradoxical aspect of our analysis: The low-temperature susceptibility depression expected in consequence of the zero-point spin reduction in the Néel state should increase for a progressively smaller interchain coupling, although at any fixed temperature the susceptibility must of course approach the result for free chains. A contradiction is avoided, however, if the depression also moves to lower temperatures, then implying merely a discontinuity at $T=0$ K at the instant when the interchain coupling vanishes; such a behavior actually resembles what has to be expected of an arbitrarily small singlet-triplet gap in the case of dimerized spin chains.[9] Nonetheless, it is reassuring that a depression in the low-temperature susceptibility is clearly visible for some ionic chain systems for which the moment reduction is significant, this being so for hexagonal $CsNiCl_3$ (Ref. 10) (where the susceptibility maximum is accessible) and $CsVCl_3$,[42] although the reduction in these cases (particularly the $S=1$ system) is perhaps not only caused by conventional zero-point fluctuation.

V. CONCLUDING REMARKS

The present single-crystal investigation of the Tl member of the thioferrate family of covalent-chain antiferromagnets by thermal neutron diffraction and SQUID susceptibility measurements confirms good quasi-1D properties and the occurrence of collinear 3D order with the moments pointing perpendicular to the chains below $T_N=196(1)$ K, and it enables an ambiguity in the moment direction to be eliminated. The steep intrachain spin-wave dispersion of the chain thioferrates has been clearly resolved, the 1D paramagnetic correlation measured, the susceptibility determined for different crystal directions, and the results subjected to a combined analysis, allowing a detailed picture of spin, exchange, and anisotropy in the Tl thioferrate to be formed.

It turns out that $TlFeS_2$ below room temperature is adequately described by standard spin-wave theory and results available in the 1D limit for a conventional antiferromagnetic Heisenberg Hamiltonian. Specifically, whereas a spin value of the free-ion order $\frac{5}{2}$ is contradicted by a noticeable Van Vleck susceptibility term as well as an unusually low ordered moment, a value $S\approx\frac{3}{2}$ is

compatible with these observations and can also consistently account for the magnitude of the magnon energies, correlation length, and susceptibility; moreover, such a model, which includes the quantum fluctuation and renormalization effects known from ionic spin chains, is clearly favored over a classical low-spin description. The analysis thus corroborates the presence of strongly covalency reduced moments in the thioferrate chains, in agreement with the delocalization expected from direct Fe contact. Yet, even though the moments may be formed by partly itinerant $3d$ electrons with no restriction to special spin values, their behavior is similar to that of localized quantum spins.

Other results underlines the role of direct Fe-Fe covalency in $TlFeS_2$. Thus an unexpectedly large spin-wave velocity of 0.54(3) eV Å is found in the chain direction, implying an extrapolated zone-boundary energy near 200 meV; the magnon energies in the thioferrate chains may therefore be the highest among quasi-1D systems to date, and the corresponding strong exchange can be largely attributed to Fe-Fe interaction. A value of the perpendicular Néel-state susceptibility somewhat lower than expected should either reflect a deviation from a local-moment behavior or indicate competitive second-neighbor interaction of roughly 12% in the chains that may again be a consequence of Fe-Fe delocalization. Last, an appreciable polarization of the $3d$ electronic shell from in-chain Fe-Fe binding is immediately visible as an anisotropy in the Van Vleck susceptibility. As a small magnon gap, on the other hand, testifies to the absence of any significant single-site or intrachain exchange anisotropy acting on the magnetic spin system, the cancellation of spin-orbit coupling in nonspherical but trivalent Fe is borne out by the data for $TlFeS_2$.

In view of the prevalence of 1D magnetic short-range order in $TlFeS_2$ throughout the investigated temperature range, the general success of a model with temperature-independent moments and exchange constants is not unexpected, and the results should be considered compatible with electronic itinerancy in the thioferrate chains. There is also no need to invoke the singlet formation predicted for exchange-dimerized local-spin chains, since an $S \approx \frac{3}{2}$ quantum spin model with zero-point fluctuation in accordance with the magnon dispersion satisfies the measured ordered moment, paramagnetic correlation, and static susceptibility. However, with the effects of dimerization being presumably small for spin values $S \gg \frac{1}{2}$ and, on the basis of data limited to temperatures far below the susceptibility maximum, presumably hard to distinguish from the effects of zero-point fluctuation, nothing can be concluded about the actual extent of exchange dimerization in $TlFeS_2$. Yet it is perhaps also not unreasonable to speculate that this quantum effect—unlike zero-point fluctuation and renormalization—is simply quenched by itinerancy.

ACKNOWLEDGMENTS

We are grateful to Y. Ito (Institute for Solid State Physics) and H. Ikeda (Ochanomizu University, Tokyo) for stimulating discussions, the allocation of instrument time, and help with the experiments. We have further benefited from comments of H. Yoshizawa and H. Kadowaki (ISSP) and Y. Endoh and K. Kakurai (Tohoku University, Sendai). The susceptibility measurements were performed at Ochanomizu University. Most of this paper was written using facilities at Tohoku University. D.W. was financially supported by the Japan Society for the Promotion of Science (JSPS).

*Present address: Hahn-Meitner-Institut, Postfach 390128, D-1000 Berlin 39, Germany.

[1]M. Zabel and K.-J. Range, Z. Naturforsch. B **34**, 1 (1979); K. Klepp and H. Boller, Monatsh. Chem. **110**, 1045 (1979).

[2]D. Welz, P. Deppe, W. Schäfer, H. Sabrowsky, and M. Rosenberg, J. Phys. Chem. Solids **50**, 297 (1989); H. Sabrowsky, M. Rosenberg, D. Welz, P. Deppe, and W. Schäfer, J. Magn. Magn. Mater. **54-57**, 1497 (1986).

[3]M. Nishi and Y. Ito, Solid State Commun. **30**, 571 (1979); Z. Tomkowicz, A. Szytula, and H. Bak-Ptasiewicz, Phys. Status Solidi A **57**, K25 (1980); W. Bronger and P. Müller, J. Less-Common Met. **100**, 241 (1984).

[4]M. Nishi, Y. Ito, and A. Ito, J. Phys. Soc. Jpn. **52**, 3602 (1983); Y. Ito, M. Nishi, C. F. Majkrzak, and L. Passell, in *Proceedings of the International Conference on Martensitic Transformations,* edited by I. Tamura (The Japan Institute of Metals, Sendai, 1987), pp. 1133–1138.

[5]M. Nishi, Y. Ito, and S. Funahashi, J. Phys. Soc. Jpn. **52**, 2210 (1983).

[6]D. Welz and M. Rosenberg, J. Phys. C **20**, 3911 (1987).

[7]W. Bronger, Z. Anorg. Allg. Chem. **359**, 225 (1968).

[8]W. Bronger and P. Müller, J. Less-Common Met. **70**, 253 (1980).

[9]J. C. Bonner and H. W. J. Blöte, Phys. Rev. B **25**, 6959 (1982); G. Spronken, B. Fourcade, and Y. Lepine, *ibid.* **33**, 1886 (1986).

[10]L. J. de Jongh and A. R. Miedema, Adv. Phys. **23**, 1 (1974), and references therein.

[11]M. Steiner, J. Villain, and C. G. Windsor, Adv. Phys. **25**, 87 (1976), and references therein.

[12]J. C. Bonner, in *Magnetostructural Correlations in Exchange Coupled Systems,* edited by R. D. Willett *et al.* (D. Reidel, Dordrecht, 1985), pp. 157–205, and references therein.

[13]M. J. Cooper and R. Nathans, Acta Crystallogr. **23**, 357 (1967); S. A. Werner and R. Pynn, J. Appl. Phys. **42**, 4736 (1971).

[14]J. A. Tarvin (unpublished); I. U. Heilmann and J. A. Tarvin (unpublished).

[15]R. E. Watson and A. J. Freeman, Acta. Crystallogr. **14**, 27 (1961).

[16]J. C. Le Guillou and J. Zinn-Justin, Phys. Rev. Lett. **39**, 95 (1977).

[17]S. K. Satija, J. D. Axe, G. Shirane, H. Yoshizawa, and K. Hirakawa, Phys. Rev. B **21**, 2001 (1980).

[18]I. U. Heilmann, J. K. Kjems, Y. Endoh, G. F. Reiter, G. Shirane, and R. J. Birgeneau, Phys. Rev. B **24**, 3939 (1981).
[19]*ISIS 1990,* annual report, edited by C. C. Wilson (Rutherford Appleton Laboratory, Chilton, Didcot, Oxfordshire, England, 1990), p. 82.
[20]F. Keffer, in *Handbuch der Physik,* edited by S. Flügge (Springer-Verlag, Berlin, 1966), Vol. XVIII/2, pp. 1–273, and references therein.
[21]W. J. L. Buyers, R. M. Morra, R. L. Armstrong, M. J. Hogan, P. Gerlach, and K. Hirakawa, Phys. Rev. Lett. **56**, 371 (1986); R. M. Morra, W. J. L. Buyers, R. L. Armstrong, and K. Hirakawa, Phys. Rev. B **38**, 543 (1988).
[22]J. Skalyo, G. Shirane, S. A. Friedberg, and H. Kobayashi, Phys. Rev. B **2**, 1310 (1970); **2**, 4632 (1970).
[23]D. C. Johnston, S. C. Mraw, and A. J. Jacobson, Solid State Commun. **44**, 255 (1982).
[24]G. Shirane, R. Nathans, O. Steinsvoll, H. A. Alperin, and S. J. Pickart, Phys. Rev. Lett. **15**, 146 (1965); M. F. Collins, V. J. Minkiewicz, R. Nathans, L. Passell, and G. Shirane, Phys. Rev. **179**, 417 (1969).
[25]M. T. Hutchings, G. Parisot, and D. Tochetti, in *Neutron Inelastic Scattering 1977* (International Atomic Energy Agency, Vienna, 1978), Vol. II, pp. 123–133.
[26]J. B. Goodenough, *Magnetism and the Chemical Bond* (Wiley, New York, 1963).
[27]T. Teranishi, J. Phys. Soc. Jpn. **16**, 1881 (1961).
[28]G. Donnay, L. M. Corliss, J. D. H. Donnay, N. Elliott, and J. M. Hastings, Phys. Rev. **112**, 1917 (1958).
[29]T. Oguchi, Phys. Rev. **133**, A1098 (1964).
[30]H. J. Zeiger and G. W. Pratt, *Magnetic Interactions in Solids* (Clarendon, Oxford, 1973).
[31]J. Kanamori and M. Tachiki, J. Phys. Soc. Jpn. **17**, 1384 (1962).
[32]S. Foner, in *Magnetism,* edited by T. Rado and H. Suhl (Academic, New York, 1963), Vol. I, pp. 383–447.
[33]P. Pincus, Phys. Rev. **113**, 769 (1959).
[34]P. L. Richards, J. Appl. Phys. **34**, 1237 (1963); A. J. Sievers and M. Tinkham, Phys. Rev. **129**, 1566 (1963).
[35]C. J. Ballhausen, *Introduction to Ligand Field Theory* (McGraw-Hill, New York, 1962); J. S. Griffith, *Theory of Transition Metal Ions* (Cambridge University Press, Cambridge, England, 1961). The spin operator can be omitted from Eq. (3) as it gives no high-frequency contribution to the susceptibility; see also J. H. Van Vleck, *The Theory of Electric and Magnetic Susceptibilities* (Oxford University Press, London, 1932).
[36]R. Kubo, Phys. Rev. **87**, 568 (1952).
[37]T. Ishikawa and T. Oguchi, Prog. Theor. Phys. **54**, 1282 (1975); see also M. E. Lines, Phys. Rev. **135**, A1336 (1964).
[38]M. T. Hutchings, E. J. Samuelsen, G. Shirane, and K. Hirakawa, Phys. Rev. **188**, 919 (1969).
[39]G. P. Gupta, D. P. E. Dickson, C. E. Johnson, and B. M. Wanklyn, J. Phys. C **10**, L459 (1977); **11**, 3889 (1978); G. P. Gupta, D. P. E. Dickson, and C. E. Johnson, *ibid.* **11**, 215 (1978).
[40]R. Sabatier, J. L. Soubeyroux, J. M. Dance, A. Tressaud, M. Wintenberger, and D. Fruchart, Solid State Commun. **29**, 383 (1979); A. Tressaud, J. L. Soubeyroux, J. M. Dance, R. Sabatier, P. Hagenmuller, and B. M. Wanklyn, *ibid.* **37**, 479 (1981).
[41]D. E. Cox and V. J. Minkiewicz, Phys. Rev. B **4**, 2209 (1971).
[42]K. Hirakawa, H. Yoshizawa, and K. Ubukoshi, J. Phys. Soc. Jpn. **51**, 1119 (1982); T. Tsuda, M. Itoh, and H. Yasuoka, *ibid.* **54**, 1599 (1985).
[43]M. Takahashi, Phys. Rev. Lett. **62**, 2313 (1989).
[44]T. Oguchi, Phys. Rev. **117**, 117 (1960).